MFI lamellae are unique among the available aluminosilicate zeolite lamellae because they have pores that run across the lamella thickness (*3*). The nanometer-scale diffusion lengths of pillared MFI and SPP allow for fast transport even for molecules with small micropore diffusivity. In this respect, pillared MFI and SPP are valuable model materials for the quantitative assessment of diffusion limitations and intrinsic kinetics. The self-etherification of benzyl alcohol in the presence of DTBP (used in order to deactivate the external sites) was considered as an example. The plot of the effectiveness factor versus the Thiele modulus shows excellent agreement with the experimental data (*23*, *29*), from which it can be concluded that Brønsted acid sites in the micropores of SPP and pillared MFI have reactivity similar to those in conventional and nanocrystalline MFI, and that the observed differences in apparent reaction rates can be fully accounted for by diffusion limitations. A comparison of effectiveness factors with that of a commercially available ZSM-5 catalyst (dashed line in Fig. 4B) reveals that 3DOm-i, pillared MFI, and SPP catalysts exhibit higher apparent reaction rates. Improved behavior of pillared MFI and SPP was also established in other reactions. For example, etherification of 5-hydroxymethyl-2-furaldehyde (HMF) to 5,5′-oxy(bismethylene)-2-furaldehyde (OBMF) proceeds to completion, whereas commercial ZSM-5 suffers from deactivation (Fig. 4C). Because OBMF is a desirable biobased intermediate (*30*), this finding underscores the potential of single–unit cell layers in applications beyond petrochemical processing.

Branching of zeolite nanometer-sized lamellae, through repetitive twinning or other intergrowth processes, is a new low-cost approach toward hierarchical materials with interconnected micropores and mesopores. It is in principle applicable to all zeolite structures that can (i) be grown anisotropically as thin layers and (ii) can support branching at certain acute angles (supplementary text and fig. S16).

References and Notes

1. A. Corma, V. Fornes, S. B. Pergher, T. L. M. Maesen, J. G. Buglass, *Nature* **396**, 353 (1998).
2. Y. X. Wang, H. Gies, B. Marler, U. Muller, *Chem. Mater.* **17**, 43 (2005).
3. K. Na *et al.*, *J. Am. Chem. Soc.* **132**, 4169 (2010).
4. W. J. Roth, D. L. Dorset, *Micropor. Mesopor. Mater.* **142**, 32 (2011).
5. M. A. Snyder, M. Tsapatsis, *Angew. Chem. Int. Ed.* **46**, 7560 (2007).
6. M. Tsapatsis, *Science* **334**, 767 (2011).
7. Z. J. Li, C. M. Lew, S. Li, D. I. Medina, Y. S. Yan, *J. Phys. Chem. B* **109**, 8652 (2005).
8. J. Pérez-Ramírez, C. H. Christensen, K. Egeblad, C. H. Christensen, J. C. Groen, *Chem. Soc. Rev.* **37**, 2530 (2008).
9. D. Liu, A. Bhan, M. Tsapatsis, S. Al Hashimi, *ACS Catal.* **1**, 7 (2011).
10. J. Wang, W. Yue, W. Zhou, M.-O. Coppens, *Micropor. Mesopor. Mater.* **120**, 19 (2009).
11. D. P. Serrano *et al.*, *Catal. Today* **168**, 86 (2011).
12. K. Na *et al.*, *Science* **333**, 328 (2011).
13. L. Manna, D. J. Milliron, A. Meisel, E. C. Scher, A. P. Alivisatos, *Nat. Mater.* **2**, 382 (2003).
14. Y.- Jun, H.-W. Chung, J.- Jang, J. Cheon, *J. Mater. Chem.* **21**, 10283 (2011).
15. T. Ohsuna, O. Terasaki, Y. Nakagawa, S. I. Zones, K. Hiraga, *J. Phys. Chem. B* **101**, 9881 (1997).
16. M. M. J. Treacy, D. E. W. Vaughan, K. G. Strohmaier, J. M. Newsam, *Proc. R. Soc. A* **452**, 813 (1996).
17. H. K. Jeong, J. Krohn, K. Sujaoti, M. Tsapatsis, *J. Am. Chem. Soc.* **124**, 12966 (2002).
18. T. Okubo *et al.*, *Angew. Chem. Int. Ed.* **40**, 1069 (2001).
19. L. Karwacki *et al.*, *Nat. Mater.* **8**, 959 (2009).
20. G. R. Millward, S. Ramdas, J. M. Thomas, *Proc. R. Soc. A* **399**, 57 (1985).
21. K. Möller, T. Bein, *Science* **333**, 297 (2011).
22. L. Y. Hou, L. B. Sand, in *Proceedings of the Sixth International Zeolite Conference*, D. Olson, A. Bisio, Eds. (Butterworths, Guildford, UK, 1983), pp. 887–893.
23. See supplementary materials on *Science* Online.
24. K. Varoon *et al.*, *Science* **334**, 72 (2011).
25. A. Tuel, Y. B. Taarit, *Micropor. Mater.* **2**, 501 (1994).
26. S. Maheshwari *et al.*, *J. Am. Chem. Soc.* **130**, 1507 (2008).
27. P. I. Ravikovitch, A. V. Neimark, *Colloids Surf. A* **187–188**, 11 (2001).
28. P. Cheung, A. Bhan, G. J. Sunley, E. Iglesia, *Angew. Chem. Int. Ed.* **45**, 1617 (2006).
29. R. Aris, in *Elementary Chemical Reactor Analysis* (Dover, Boston, 1989), chap. 6.
30. O. Casanova, S. Iborra, A. Corma, *J. Catal.* **275**, 236 (2010).

Acknowledgments: We acknowledge support, for all aspects of SPP zeolite, from the Catalysis Center for Energy Innovation (award DESC00001004), an Energy Frontier Research Center funded by the U.S. Department of Energy, Office of Science, Office of Basic Energy Sciences. Partial support for synthesizing conventional, 3DOm-i, and pillared zeolites and their catalytic testing was provided by ADMIRE (Abu Dhabi–Minnesota Institute for Research Excellence), NSF Emerging Frontiers in Research and Innovation grant 0937706, and the Initiative for Renewable Energy and the Environment, a program of the University of Minnesota's Institute on the Environment. Portions of this work were conducted at the University of Minnesota Characterization Facility, which receives partial support from NSF through the NNIN program. Computing resources were provided by the Minnesota Supercomputing Institute. Supported by a University of Minnesota Graduate School doctoral dissertation fellowship (X.Z.) and by ADGAS and GASCO (Y.A.W.). We thank T. Ohsuna for helpful suggestions and S. Hwang for obtaining solid-state NMR spectra. M.T. has an equity interest in, and serves as the Chief Scientific Officer for, Argilex, a company that may commercially benefit from the results of this research. M.T., X.Z., and the University of Minnesota have financial interests arising from a right to receive royalty income under the terms of a license agreement with Argilex. These relationships have been reviewed and managed by the University of Minnesota in accordance with its conflict of interest policies. A U.S. patent application by M.T. and X.Z. was filed on 3 November 2011 (Application No. 13/288,595).

Supplementary Materials

www.sciencemag.org/cgi/content/full/336/6089/1684/DC1
Materials and Methods
Supplementary Text
Figs. S1 to S16
Tables S1 and S2
References (*31*–*40*)

27 December 2011; accepted 8 May 2012
10.1126/science.1221111

Seemingly Anomalous Angular Distributions in H + D_2 Reactive Scattering

Justin Jankunas,[1] Richard N. Zare,[1]* Foudhil Bouakline,[2] Stuart C. Althorpe,[3] Diego Herráez-Aguilar,[4] F. Javier Aoiz[4]

When a hydrogen (H) atom approaches a deuterium (D_2) molecule, the minimum-energy path is for the three nuclei to line up. Consequently, nearly collinear collisions cause HD reaction products to be backscattered with low rotational excitation, whereas more glancing collisions yield sideways-scattered HD products with higher rotational excitation. Here we report that measured cross sections for the H + D_2 → HD(v' = 4, j') + D reaction at a collision energy of 1.97 electron volts contradict this behavior. The anomalous angular distributions match closely fully quantum mechanical calculations, and for the most part quasiclassical trajectory calculations. As the energy available in product recoil is reduced, a rotational barrier to reaction cuts off contributions from glancing collisions, causing high-j' HD products to become backward scattered.

It is tempting and even at times quite insightful to describe the dynamics of chemical reactions in simple terms of classical billiard-ball collisions. In this picture, the impact parameter is defined as the distance of closest approach of the centers of the two billiard balls if they could travel without interaction in straight lines. Consider what happens when a billiard ball strikes another at rest. For a head-on collision, corresponding to zero impact parameter, the incoming billiard ball recoils backward in the center-of-mass frame. For a glancing collision between the two billiard balls, corresponding to a larger impact parameter, the incoming ball is scattered more sideways with respect to its initial direction. Next, consider the more complicated case of an atom A colliding with a diatomic molecule BC at rest to form by direct reaction the products AB and C. Furthermore, let us suppose that the

[1]Department of Chemistry, Stanford University, Stanford, CA 94305–5080, USA. [2]Institut für Chemie, Universität Potsdam, Karl-Liebknecht-Strasse 24-25, 14476 Potsdam-Golm, Germany. [3]Department of Chemistry, University of Cambridge, Lensfield Road, Cambridge CB2 1EW, UK. [4]Departamento de Química Física, Facultad de Química, Universidad Complutense, 28040 Madrid, Spain.

*To whom correspondence should be addressed. E-mail: zare@stanford.edu

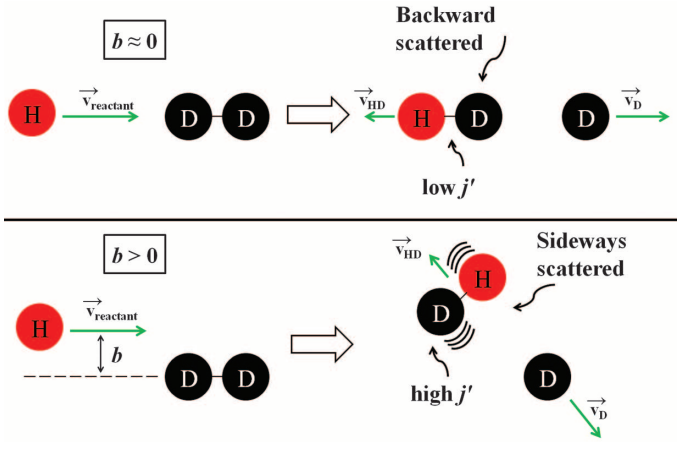

Fig. 1. Cartoon depicting a hypothetical H + D_2 → HD(v', j') + D reactive scattering event. $\vec{v}_{reactant}$ denotes the initial relative velocity of the reagents, and $\vec{v}_{HD}$ and $\vec{v}_D$ are the corresponding velocities of the HD and D products in the center-of-mass frame. The impact parameter b is defined as the distance of closest approach between the H atom and the center-of-mass of the D_2 molecule in the absence of interaction. Reactive collisions with small b lead to backward-scattered HD products in states of low rotational excitation (upper panel), whereas reactive collisions with large b lead to sideways-scattered HD products with high rotational excitation (lower panel).

preferred approach geometry for reaction is collinear, that is, with all three nuclei in a straight line. Under these conditions, it is natural to expect that for small impact parameters, the AB product of the direct reaction rebounds backward with little rotational excitation, whereas for larger impact parameters the AB product becomes increasingly sideways scattered with more rotational excitation (*1*, *2*). Indeed, this behavior has described all previous studies of direct [i.e., non–time-delayed (*3*, *4*)], collinear bimolecular reactions, including the benchmark reaction system H + D_2 → HD + D (*5*–*10*). Figure 1 illustrates schematically the impact parameter and other useful concepts for the H + D_2 → HD(v',j') + D reaction, where v' and j' are the vibrational and rotational quantum numbers, respectively, and the data in figs. S1 and S2 manifest the expected trend for the H + D_2 → HD(v' = 1, j') + D and H + D_2 → HD(v' = 3, j') + D reactions, respectively,

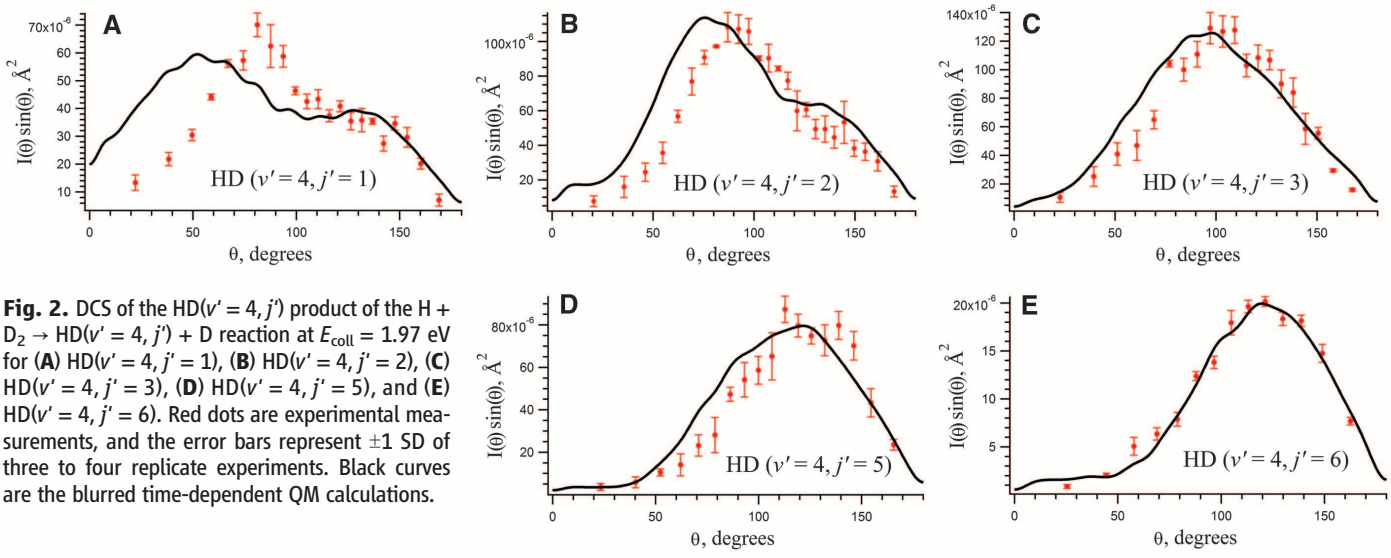

Fig. 2. DCS of the HD(v' = 4, j') product of the H + D_2 → HD(v' = 4, j') + D reaction at E_{coll} = 1.97 eV for (**A**) HD(v' = 4, j' = 1), (**B**) HD(v' = 4, j' = 2), (**C**) HD(v' = 4, j' = 3), (**D**) HD(v' = 4, j' = 5), and (**E**) HD(v' = 4, j' = 6). Red dots are experimental measurements, and the error bars represent ±1 SD of three to four replicate experiments. Black curves are the blurred time-dependent QM calculations.

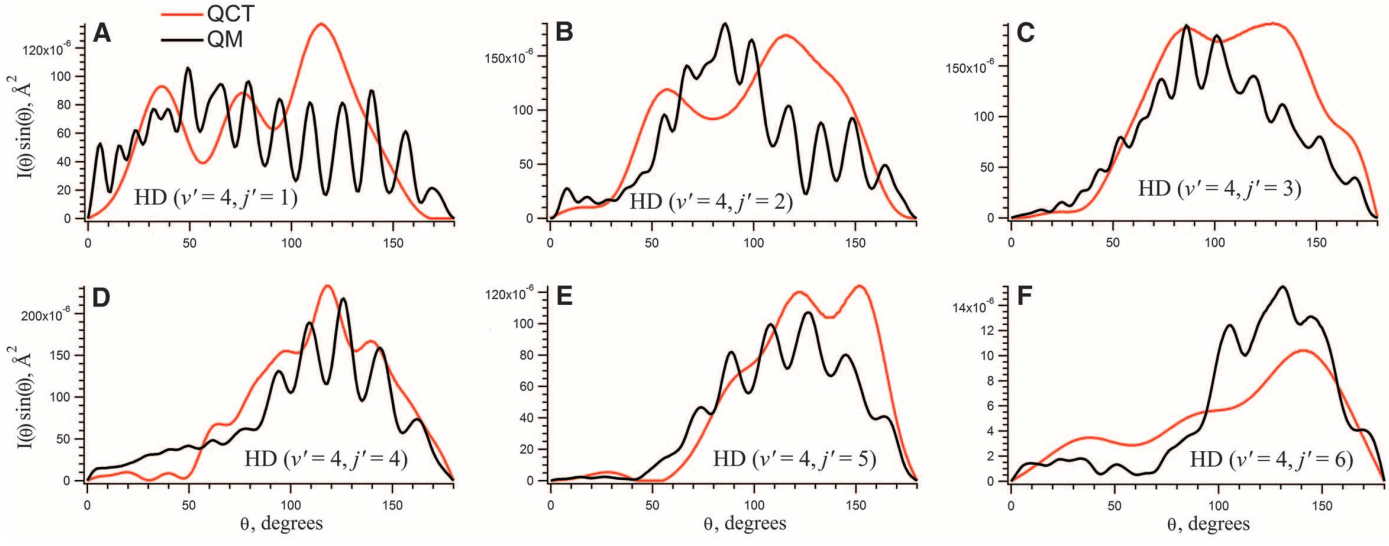

Fig. 3. Comparison between QCT (red curves) and unblurred time-independent QM (black curves) calculations for (**A**) HD(v' = 4, j' = 1), (**B**) HD(v' = 4, j' = 2), (**C**) HD(v' = 4, j' = 3), (**D**) HD(v' = 4, j' = 4), (**E**) HD(v' = 4, j' = 5), and (**F**) HD(v' = 4, j' = 6).

both at a collision energy of E_{coll} = 1.97 eV. This behavior has become one of the celebrated rules of reaction dynamics and encourages the belief that the classical motion of the nuclei on the ABC potential energy surface governs the reactive collision outcome when quantum tunneling effects are disregarded. Imagine, then, our initial surprise to find the opposite behavior for the reaction $H + D_2 \rightarrow HD(v' = 4, j') + D$ at E_{coll} = 1.97 eV in which with increasing product rotational excitation, the angular distribution of HD(v' = 4, j') increasingly shifts to the backward direction. Moreover, we show, experimentally and theoretically, that such anomalous angular distributions are general and to be expected for any direct collinear bimolecular reaction as the energy available for product recoil is reduced.

We employed a three-dimensional ion imaging apparatus (*11*) using the photoloc technique to record the differential cross section (DCS) of the HD(v' = 4, j') molecules in the same way we have studied the other H + D_2 reactions. In brief, a mixture of 1 to 3% HBr in D_2 was introduced through a 10-Hz pulsed valve into a vacuum chamber. The reactants underwent internal and translational cooling in a supersonic expansion, and almost all the D_2 was prepared in (v = 0, $j \leq 2$) internal states. Reaction was initiated by photolyzing HBr at 199 nm to produce fast H atoms. The resulting HD products were state-selectively ionized via [2+1] resonance-enhanced multiphoton ionization. As can be seen from Fig. 2, as the rotational excitation of the HD(v' = 4, j') increases, the DCS shifts in a backward direction. Fully quantum mechanical (QM) calculations were carried out using the wave-packet method of Althorpe (*12*), in which a quantum wave packet, containing a spread of desired energies, is propagated from the initial (H + D_2) to the final (HD + D) arrangements of the reaction, on the potential energy surface of Boothroyd–Keogh–Martin–Peterson (*13*). Time-independent QM calculations were also carried out at specific collision energies using the ABC code (*14*). The results are virtually identical to those obtained with the wave-packet calculations. We blurred the resulting DCSs (*10*) to account for the spread in the rotational levels of the D_2 reagent, the spread caused by imperfect translational cooling in the supersonic beam expansion, and the spread resulting from the finite instrument angular resolution. Figure 2 shows that each blurred DCS closely matches the corresponding experimental measurement, engendering confidence that the anomalous angular distributions reported here are accurate. The only disagreement occurs in the forward scattering direction for HD(v' = 4, j' = 1), for which we presently have no explanation. Data are not reported for HD(v' = 4, j' = 0) and HD(v' = 4, j' = 4) because of too much background interference for the wavelengths used to detect these reaction products.

To seek an explanation for this behavior, we performed quasiclassical trajectory (QCT) calculations on the same potential energy surface. To avoid the assignment of quantum numbers of states that are energetically inaccessible, we used the Gaussian binning procedure (*15*–*17*). Briefly, this entailed weighting each trajectory according to Gaussian functions centered on the correct QM vibrational action in such a way that the closer the (real) vibrational quantum number of one trajectory was to the nearest integer, the larger was the weight assigned to that trajectory. A batch of 15 million trajectories was run at 1.97-eV collision energy with a maximum impact parameter of 1.3 Å. Figure 3 presents a comparison of the unblurred fully quantum and the QCT results. Overall, the QCT calculations illustrate the same anomalous trend of increasing backward scattering with increasing rotational excitation of the HD(v' = 4, j') product, but some notable disagreements are apparent for HD(v' = 4, j' = 1 and 2). Such disagreements between quantum and QCT are to be expected because the recoil energy of the products ensures that the de Broglie wavelength of the separating particles is large in comparison with the dimensions of the collision process, and hence the semiclassical assumptions behind the QCT approach start to break down. The rapid oscillations (with a period of ~10°) in the quantum cross sections are the result of nearside-farside interference between products scattering into opposite hemispheres (*18*). The deviations between QCT and QM calculations seem most pronounced for HD(v' = 4, j' = 1, 2, and 6) so that the disagreement does not simply scale with increasing de Broglie wavelength.

We suggest that the anomalous angular distributions arise from the existence of a centrifugal barrier in the reaction path that impedes radial motion, leading to products with a high degree of internal excitation. Before collision, the relative velocity $\vec{v}$ of the approaching H and D_2 is perpendicular to the direction of the impact parameter b (see Fig. 1), and hence the magnitude of the total angular momentum of the colliding system is given by $L = \mu v b$, where μ is the reduced mass of the collision partners. Consequently, at a radial distance R between the reactants, the centrifugal energy is given by $L^2/2\mu R^2 = J(J+1)\hbar^2/2\mu R^2 = \frac{1}{2}\mu b^2 v^2/R^2 = E_{coll} b^2/R^2$, ignoring the small amount of angular momentum associated with D_2 rotation. Thus, as H and D_2 draw closer, R decreases and more energy of motion becomes bound up in centrifugal energy. Let $P(J)$ be the probability of reaction to produce the HD product in the internal state (v', j'). The cross section to produce HD(v', j') is found by summing $P(J)$ weighted by $(2J + 1)$ over all possible J values that contribute to this process. Note that J is proportional to the impact parameter b. As J increases, more of the HD(v', j') product becomes side scattered, but also more energy is bound up in the centrifugal energy

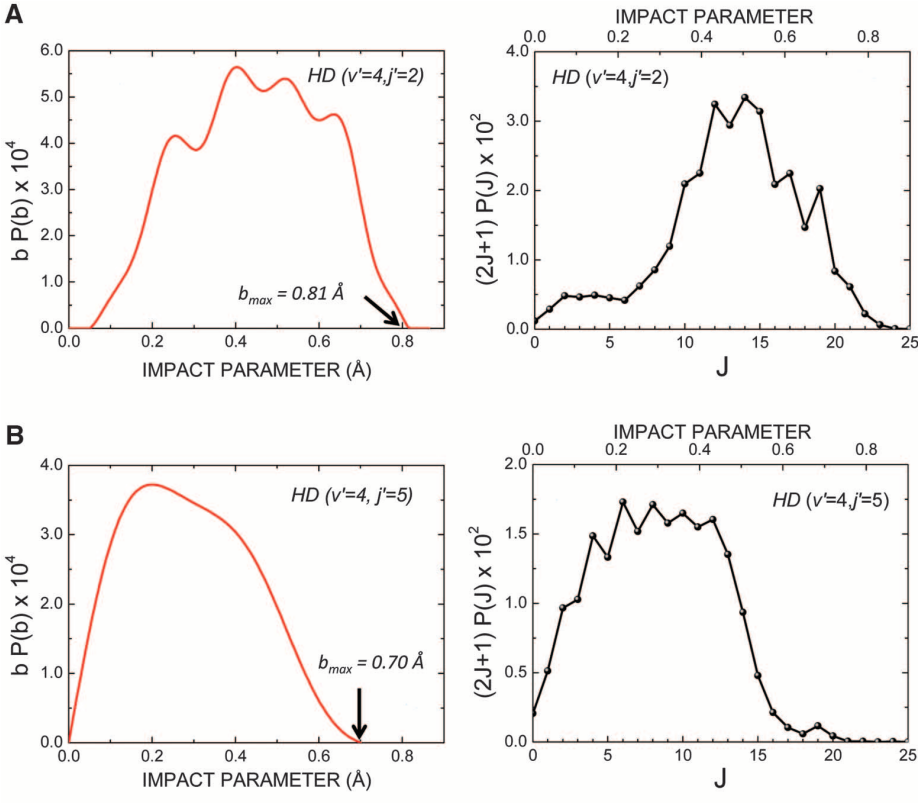

Fig. 4. Plots of the time-independent QM-derived $P(J)(2J + 1)$ versus J and the QCT-derived $bP(b)$ versus b for (**A**) HD(v' = 4, j' = 2) and (**B**) HD(v' = 4, j' = 5) for the reaction H + D_2 → HD(v' = 4, j') + D at a collision energy of 1.97 eV. As rotational excitation of the HD product increases, the contributions to the cross section from $P(J)(2J + 1)$ and $bP(b)$ for larger values of J and b diminish, causing backscattering of the HD(v' = 4, j') product.

and not available for radial motion to bring H and D_2 closer together for reaction to occur to produce the HD(v', j') product state. That is, for HD(v', j') products where most of the available energy is in internal excitation, H + D_2 collisions with high impact parameters (high J values) contribute less to product formation than those with low b values (low J values). Thus, as rotational excitation of the HD(v', j') product increases for a given fixed total collision energy, this product will at some point become more backscattered than an HD(v', j') product with somewhat less rotational excitation.

This explanation is supported by examining the form of $(2J+1)\,P(J)$ and $bP(b)$ for HD($v'=4$, $j'=2$) (Fig. 4A) and HD($v'=4$, $j'=5$) (Fig. 4B). Both QM and QCT plots show the same overall behavior. The exact details depend on the form of the potential energy surface, but we expect this phenomenon to be general. It is not surprising, then, to find that the H + D_2 → HD($v'=3$, $j'=8$ and 10) + D reactions at 1.97 eV show the same behavior as seen for HD($v'=4$, j'), as shown in fig. S3. We expect that this seemingly anomalous behavior will apply to other direct bimolecular reactions in which most of the energy of reaction becomes tied up in the internal motions of the reaction products.

References and Notes

1. R. D. Levine, *Molecular Reaction Dynamics* (Cambridge Univ. Press, Cambridge, UK, 2005).
2. P. Casavecchia, K. Liu, X. Yang, in *Tutorials in Molecular Reaction Dynamics*, M. Brouard, C. Vallance, Eds. (RSC, Cambridge, UK, 2010), p. 175.
3. S. C. Althorpe *et al.*, *Nature* **416**, 67 (2002).
4. S. A. Harich *et al.*, *Nature* **419**, 281 (2002).
5. E. Wrede *et al.*, *J. Chem. Phys.* **110**, 9971 (1999).
6. F. Fernández-Alonso *et al.*, *J. Chem. Phys.* **115**, 4534 (2001).
7. B. D. Bean, J. D. Ayers, F. Fernandez-Alonso, R. N. Zare, *J. Chem. Phys.* **116**, 6634 (2002).
8. F. J. Aoiz, L. Bañares, V. J. Herrero, *Int. Rev. Phys. Chem.* **24**, 119 (2005).
9. K. Koszinowski *et al.*, *J. Chem. Phys.* **127**, 124315 (2007).
10. N. C.-M. Bartlett *et al.*, *Phys. Chem. Chem. Phys.* **13**, 8175 (2011).
11. K. Koszinowski, N. T. Goldberg, A. E. Pomerantz, R. N. Zare, *J. Chem. Phys.* **125**, 133503 (2006).
12. S. C. Althorpe, *J. Chem. Phys.* **114**, 1601 (2001).
13. A. I. Boothroyd, W. J. Keogh, P. G. Martin, M. R. Peterson, *J. Chem. Phys.* **104**, 7139 (1996).
14. D. Skouteris, J. F. Castillo, D. E. Manolopoulos, *Comput. Phys. Commun.* **133**, 128 (2000).
15. L. Bonnet, J.-C. Rayez, *Chem. Phys. Lett.* **277**, 183 (1997).
16. L. Bañares, F. J. Aoiz, P. Honvault, B. Bussery-Honvault, J.-M. Launay, *J. Chem. Phys.* **118**, 565 (2003).
17. L. Bonnet, J.-C. Rayez, *Chem. Phys. Lett.* **397**, 106 (2004).
18. A. J. Dobbyn, P. McCabe, J. N. L. Connor, J. F. Castillo, *Phys. Chem. Chem. Phys.* **1**, 1115 (1999).

Acknowledgments: We gratefully acknowledge funding support from the U.S. National Science Foundation (grant NSF CHE-1025960 to J.J. and R.N.Z.), the Alexander von Humboldt Foundation (F.B.), the UK Engineering and Physical Sciences Research Council (S.C.A.), and the Spanish Ministry of Science and Innovation (MCINN) (grants CTQ2008-02578 and CSD2009-00038 to F.J.A. and D.H.). D.H. acknowledges the FPU fellowship AP2009-0038.

Supplementary Materials

www.sciencemag.org/cgi/content/full/336/6089/1687/DC1
Figs. S1 to S3

1 March 2012; accepted 19 April 2012
10.1126/science.1221329

Major Earthquakes Occur Regularly on an Isolated Plate Boundary Fault

Kelvin R. Berryman,[1]* Ursula A. Cochran,[1] Kate J. Clark,[1] Glenn P. Biasi,[2] Robert M. Langridge,[1] Pilar Villamor[1]

The scarcity of long geological records of major earthquakes, on different types of faults, makes testing hypotheses of regular versus random or clustered earthquake recurrence behavior difficult. We provide a fault-proximal major earthquake record spanning 8000 years on the strike-slip Alpine Fault in New Zealand. Cyclic stratigraphy at Hokuri Creek suggests that the fault ruptured to the surface 24 times, and event ages yield a 0.33 coefficient of variation in recurrence interval. We associate this near-regular earthquake recurrence with a geometrically simple strike-slip fault, with high slip rate, accommodating a high proportion of plate boundary motion that works in isolation from other faults. We propose that it is valid to apply time-dependent earthquake recurrence models for seismic hazard estimation to similar faults worldwide.

A long-standing acceptance of Reid's (*1*) elastic rebound theory of earthquakes combined with the knowledge that tectonic plates move steadily over geological time scales has led to an appealing—but rarely demonstrated—idea that major earthquakes on plate boundary faults occur relatively regularly (*2*–*5*). In contrast, several studies have suggested that faults rupture randomly or produce temporal clusters of earthquakes in response to various complexities, including fault interactions (*6*–*9*). The increasing popularity of models of random or clustered earthquake recurrence may reflect the paucity of earthquake histories from geometrically simple, rapidly slipping, isolated plate boundary faults. Paleoseismology provides evidence for the timing, size, and location of past major earthquakes on faults over longer time periods than the historical record, improving understanding of fault behavior and enabling estimates of future earthquake occurrence to be made (*5*, *7*, *9*, *10*).

We present a long earthquake record determined using paleoseismological techniques from the Alpine Fault in southwest New Zealand to assess the relationship between fault characteristics and patterns of earthquake recurrence. The Alpine Fault is ~850 km long and slips horizontally at average rates ranging from 14 mm/year in the north (*11*) to 31 mm/year in the south (*12*), with a subordinate amount of vertical slip (Fig. 1, A and B), making it one of the longest, straightest, and fastest-moving plate boundary transform faults on Earth. In the southwestern South Island, the Alpine Fault accommodates two-thirds of the relative motion between the Pacific and Australian tectonic plates (Fig. 1, A and B) (*13*, *14*). The remainder is accommodated by distributed deformation across the width of the plate boundary in the South Island (*13*–*15*). No major earthquake has occurred on the Alpine Fault since written records began (~170 years ago), but various lines of evidence indicate that the fault ruptures in large [moment magnitude (M_w) > 7] to possibly great (M_w > 8) earthquakes (*16*) and poses a substantial seismic hazard. Previous paleoseismic work has provided age constraints for the past four surface-rupturing earthquakes (*17*–*21*), but this yields only three interseismic intervals with which to assess the Alpine Fault's recurrence behavior. We extend the known record to a total of 24 major earthquakes over the past 8000 years at Hokuri Creek on the southern onshore section of the fault (Fig. 1C).

The formation and exposure of a long, fault-proximal, sedimentary earthquake record at Hokuri Creek is the result of specific geomorphological conditions. Hokuri Creek used to flow across the Alpine Fault through what is now an abandoned gorge (Fig. 1C). Holocene sediments accumulated against the fault over a 20-ha area adjacent to the creek to a total section thickness of 18 m (fig. S1). Deposition ceased when the creek changed course and flowed along the fault instead of across it at ~1000 C.E., before the penultimate Alpine Fault earthquake. Rapid incision around the junction of the north and south branches of Hokuri Creek has since exposed the sediments (Fig. 1C) (*22*). The sedimentary section comprises decimeter-thick beds of alternating shallow-water peat and silt units. Geomorphological investigations reveal that this cyclic stratigraphy is bounded to the northwest by the main scarp of the Alpine Fault.

Geologic and paleoenvironmental investigations indicate that the mechanism for formation of the cyclic peat-silt stratigraphy depends on surface rupture of the Alpine Fault. At the Hokuri

[1]GNS Science, Post Office Box 30-368, Lower Hutt 5040, New Zealand. [2]Seismological Laboratory, University of Nevada-Reno, Reno, NV 89557, USA.

*To whom correspondence should be addressed E-mail: k.berryman@gns.cri.nz